J Mater Sci (2008) 43:1214–1219
DOI 10.1007/s10853-007-2287-1

# Synthesis of europium-doped yttrium hydroxide and yttrium oxide nanosheets

**Atsuya Towata · Manickam Sivakumar · Kyuichi Yasui · Toru Tuziuti · Teruyuki Kozuka · Yasuo Iida**

Received: 30 October 2006 / Accepted: 31 October 2007 / Published online: 4 December 2007


**Abstract** A new approach has been developed for the preparation of $Y(OH)_3$:Eu and $Y_2O_3$:Eu nanosheets using the sol–gel method and hydrothermal reactions. XRD patterns showed that the product was purely hexagonal-phase $Y(OH)_3$. TEM images revealed that the nanosheets are square shaped ($1 \times 1$ $\mu m^2$) with a thickness of several tens of nanometers. In addition, it was found that cubic-phase $Y_2O_3$ nanosheets can be obtained by calcination of $Y(OH)_3$ at 900 °C for 1 h. More importantly, the thus-prepared $Y(OH)_3$:Eu and $Y_2O_3$:Eu nanosheet phosphors were found to exhibit a relatively high photoluminescence (PL) intensity.

## Introduction

Phosphors are technologically important materials for display applications. The most important properties for such applications are high luminance and long life. Activated oxide phosphors doped by rare earth elements are investigated extensively in order to make the enhancement of the luminescence. Europium-doped yttria ($Y_2O_3$:Eu) is an efficient red-emission phosphor and has been used in fluorescent lights (FL) and cathode ray tubes (CRT) [1]. Recent studies show that $Y_2O_3$:Eu nanoparticles have significant promise in field emission displays (FED) and plasma display panels (PDP) [2, 3].

A variety of methods have been used to prepare $Y_2O_3$-based phosphors, such as precipitation [4–6], sol–gel processing [7], hydrothermal treatment [8], solvothermal treatment [9], chemical vapor deposition [10], spray pyrolysis [11, 12], and combustion synthesis [13, 14].

Laminating materials consisting of plate-like particles have been used for various applications. For example, scattering is suppressed and transparency improves in the case of optical materials because the space between plate-like particles is smaller than that between spherical particles. It is thought that plate-like particles could be used to fabricate grain-oriented ferroelectric ceramics [15, 16]. Plate-like particles are required to enhance the shielding capability of inorganic UV-shielding materials [17].

It is possible to produce a transparent and smooth film by using nanosheet phosphors. In this article, we report the preparation of yttrium hydroxide and yttrium oxide nanosheets doped with europium, as well as their crystalline and fluorescent characteristics.

## Experimental

Yttrium isopropoxide (YIP) (Kojundo Chemical Lab Co., Ltd.) was used as a source of yttrium hydroxide, europium (III) chloride hexahydrate ($EuCl_3 \cdot 6H_2O$) was used as a source of europium, and ethylene glycol monoisopropyl ether (EGME) (Wako Pure Chemical Industries, Ltd.) was used as a stabilizer.

The reagent compositions and the synthesis procedure were as follows: First, YIP and $EuCl_3 \cdot 6H_2O$ were added to EGME and agitated for 12 h. Next, the solution was mixed in water and stirred. The mixture was then added in a Teflon

A. Towata (✉) · K. Yasui · T. Tuziuti · T. Kozuka · Y. Iida
National Institute of Advanced Industrial Science and Technology (AIST), 2266-98 Anagahora, Shimoshidami, Moriyama-ku, Nagoya 463-8560, Japan
e-mail: a.towata@aist.go.jp

M. Sivakumar
Bharathidasan Institute of Technology, Bharathidasan University, Trichy 620 024, India

pressure vessel. The vessel was sealed and placed in an oven at 180 °C for 6 h. After cooling, the synthesized powder was washed three times with ethanol and water, followed by centrifugation of the resulting solution, and then dried.

The crystalline phase analysis of the synthesized $Y(OH)_3$ powders was performed using X-ray diffractometry (XRD; Model RINT-2550/PC, Rigaku Co., Japan) with CuKα radiation. Thermogravimetric analysis (TG) and differential thermal analysis (DTA) were performed using a simultaneous micro-DTA/TG apparatus (Model 2020S MK12, MAC Science) to study the phase transition. For this purpose, samples were accurately weighed to five decimal places in a platinum crucible and weight losses were recorded from 25–1,000 °C under ambient pressure at a heating rate of 10 °C/min and by using α-alumina as a reference. FT-IR spectra of the synthesized powders, as KBr pellets, were taken using FTIR-8400S spectrophotometer (SHIMADZU) in the range of 400–4,000 $cm^{-1}$. Powder morphology was determined by using a JEOL JM-5600N scanning electron microscope (SEM) and HITACHI S-4300 field emission scanning electron microscope and a JEOL JEM-2010 transmission electron microscope (TEM) operating at 200 kV. Energy dispersive X-ray spectroscopy (EDS) was used for compositional analyses. A HITACHI F-4500 Spectrofluorometer equipped with a 150-W Xe arc lamp was used for photoluminescence (PL) measurements at room temperature. The sample loaded on the powder holder provided by HITACHI was mounted at about 45° to the excitation and source for PL measurement.

## Results and discussion

An SEM micrograph and X-ray diffraction of the sample synthesized with EGME are shown in Figs. 1 and 2, respectively. It can be seen that the particles are nanosheets and that some are thicker at the center. The nanosheets are square shaped, 1–1.5 μm on each side, some of them lacking corners. The nanosheets are several tens of nanometers thick, and some of them overlap with each other. The crystal structure is confirmed to be hexagonal yttrium hydroxide, and the (100) peak is more intense than the standard peak given in the JCPDS data file (#83-2042). This is why the particles were laminated and well oriented in the shape of nanosheets. There is also an intense peak at 12°, which may be due to the presence of organic materials.

For comparison, a hydrothermal reaction without EGME was also carried out. The SEM micrograph and X-ray diffraction of the sample synthesized without EGME are shown in Figs. 3 and 4, respectively. It can be seen that the $Y(OH)_3$ products are almost rods and fibers, with diameters ranging from 50 to 800 nm, and are several micrometers long. The observed diffraction peaks could be indexed to

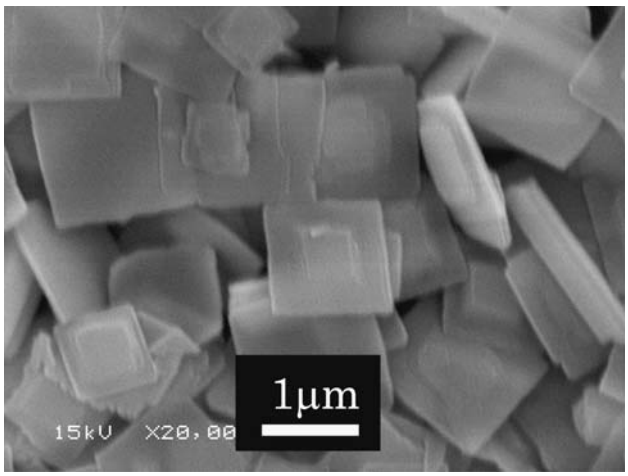


**Fig. 1** SEM micrograph of the sample synthesized with ethylene glycol monoisopropyl ether (EGME)

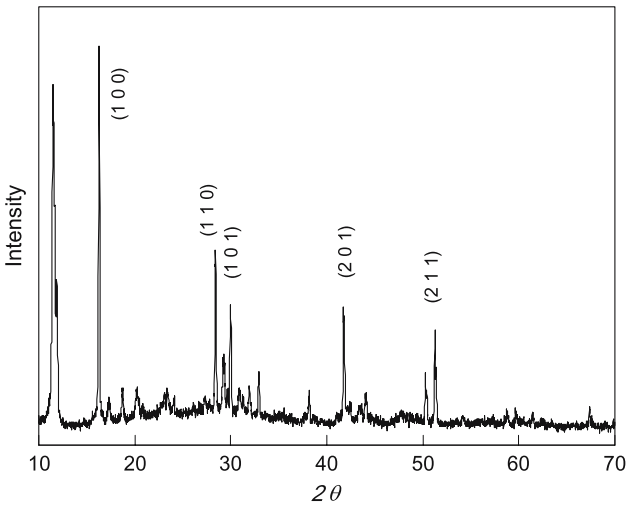


**Fig. 2** Powder XRD pattern of the sample synthesized with EGME

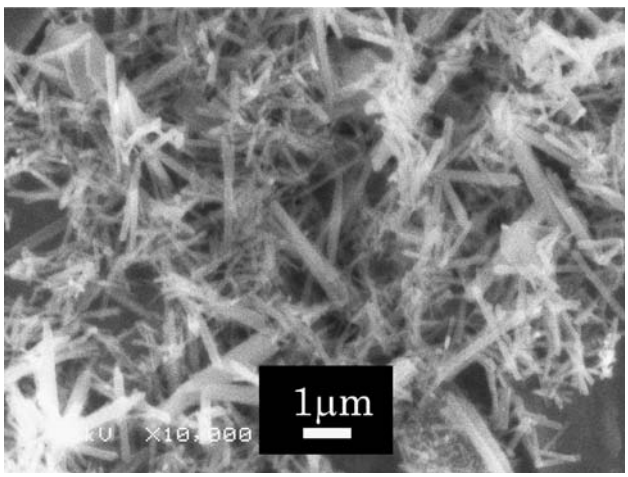


**Fig. 3** SEM micrograph of the sample synthesized without EGME

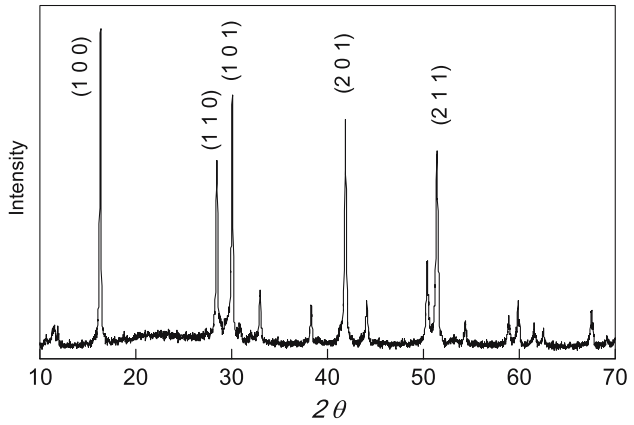


**Fig. 4** Powder XRD pattern of the sample synthesized without EGME

the hexagonal phase. In the case of the sample without EGME, the particles have been progressing by anisotropic growth so that rare earths have been detected frequently [18]. Using the sol–gel method, many oriented films have been synthesized with organic ligands. Nishide et al. [19] reported that sol–gel processes involving a specific organic additive produce oriented crystals in films grown on amorphous substrates. They also reported fabricating strongly oriented $Y_2O_3$ films by the sol–gel process using 2-(2-methoxyethoxy) ethanol (MEE). Inoue et al. [20] found that the thermal treatment of crystalline aluminum hydroxide in an ethylene glycol medium yielded a novel derivative of boehmite, in which the ethylene glycol moiety was incorporated into the boehmite layers. Thus, in the case of the sample with EGME, the OH of EGME may be used as a planar template and the particles grow flat.

Thermal analysis of the nanosheets (Fig. 5) reveals the crystal-phase transitions. It can be seen that the first phase transition, which is due to the loss of water molecules bound to the particles, occurred below 200 °C. In the DTA curve, we can observe endothermic peaks at 305 °C and 411 °C. At the same temperatures, weight loss was observed in the TG curves. Sato et al. [21] have found that hexagonal $Y(OH)_3$ transformed into YOOH at 300 °C via the reaction $Y(OH)_3 \rightarrow YOOH + H_2O$, and into $Y_2O_3$ at 450 °C via $2YOOH \rightarrow Y_2O_3 + H_2O$. In our case, the endothermic peaks appeared at almost the same temperatures, confirming that the same phase transitions took place. These peaks can be attributed to partial dehydroxylation. The dehydroxylation reaction continues up to 1,000 °C. The FTIR spectrum of the particles (Fig. 6) shows a peak at 1,535 $cm^{-1}$, which could be assigned to stretching of the C–C bond. The appearance of peaks at 1,367 and 3,030 $cm^{-1}$ is mainly attributed to bending and stretching of the C–H bond, respectively. Thus, it can be concluded that the sample contains residual organic matter derived from YIP and EGME. However, no exothermic reaction peaks could be observed in the DTA curve. The absence of exothermic peaks could be attributed to the fact that although an exothermic reaction occurred from 200 to 500 °C, its presence was masked by one of the endothermic peaks associated with dehydroxylation [22].

The SEM micrograph and X-ray diffraction pattern of the samples heated at 900 °C for 1 h are shown in Figs. 7 and 8, respectively. The heat-treated particles retained their nanosheet structure. It can be seen that $Y_2O_3$ are in the form of rods and fibers, which have slightly shrunk in diameter compared to the hydroxide. The size of the heat-treated particles is comparable to that of the particles before heating. During the decomposition process, hexagonal $Y(OH)_3$ gradually transforms into cubic $Y_2O_3$. However, the phase transformation into the cubic phase does not result in the collapse of the nanosheets into particles. A similar phenomenon has been observed in other

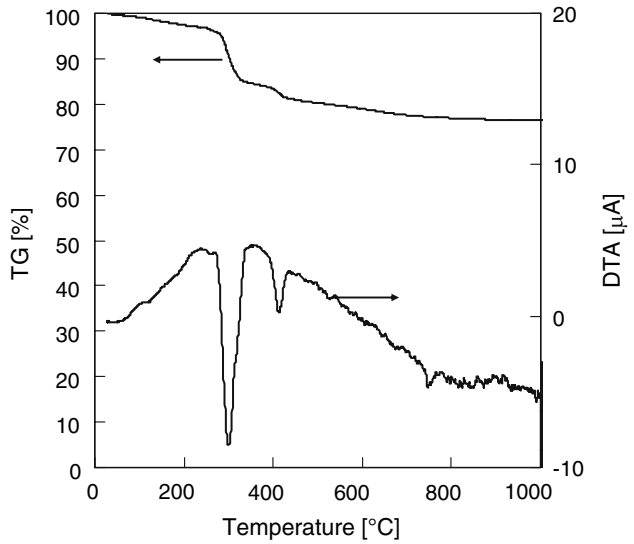


**Fig. 5** TG-DTA curves of the sample synthesized with EGME

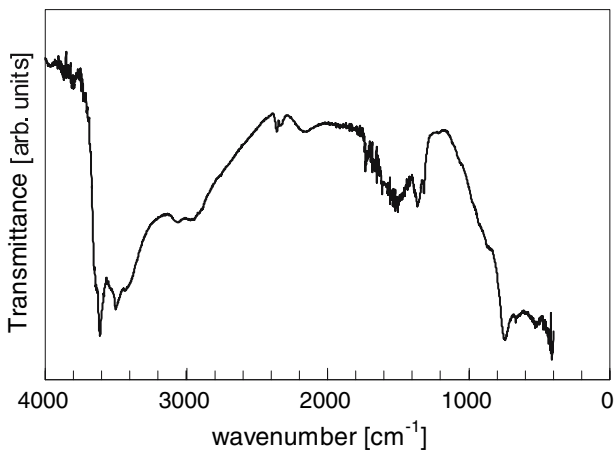


**Fig. 6** FTIR spectrum of the sample synthesized with EGME

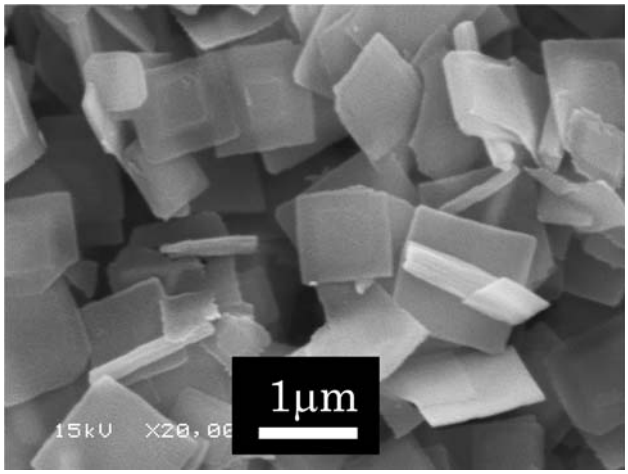


**Fig. 7** SEM micrograph of the sample obtained by heat treatment at 900 °C for 1 h in air

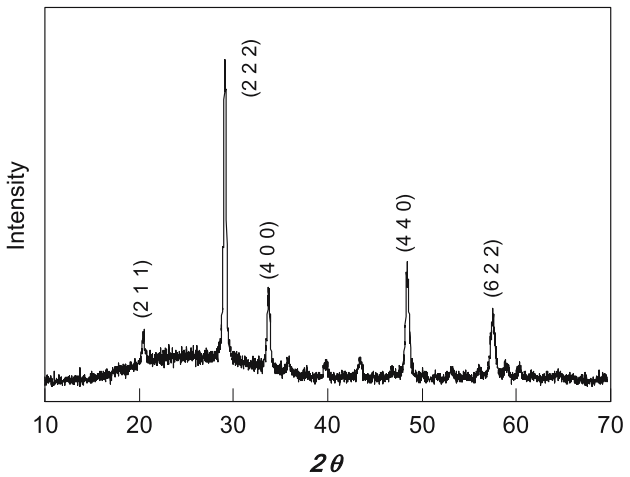


**Fig. 8** Powder XRD pattern of the $Y_2O_3$ nanosheets obtained by heat treatment at 900 °C for 1 h in air

studies [23, 24], e.g., Tang reported that such a transformation was common for rare earth compound decomposition. The crystal structure is cubic $Y_2O_3$. TEM observation (Fig. 9) indicates that these particles consist of randomly oriented, very fine nanocrystallites. The micrograph reveals the presence of lattice defects, such as dislocations and twin boundaries, in the nanosheets. The nanosheet content, as determined by EDX analysis, shows that Y:Eu = 87.8:11.2 wt.%. This content is almost the same as that of the addition content (YIP 0.25 mol/L, $EuCl_3{\cdot}6H_2O$ 0.018 mol/L).

The SEM micrograph of the sample synthesized under a YIP concentration of 3.75 mol/L is shown in Fig. 10. In the case of the more concentrated yttrium solution, some sheets grew to 5 μm. In the ordinary hydrothermal reaction, the particle size was small because the rate of nucleation was higher than that of grain growth, and thus, the number of

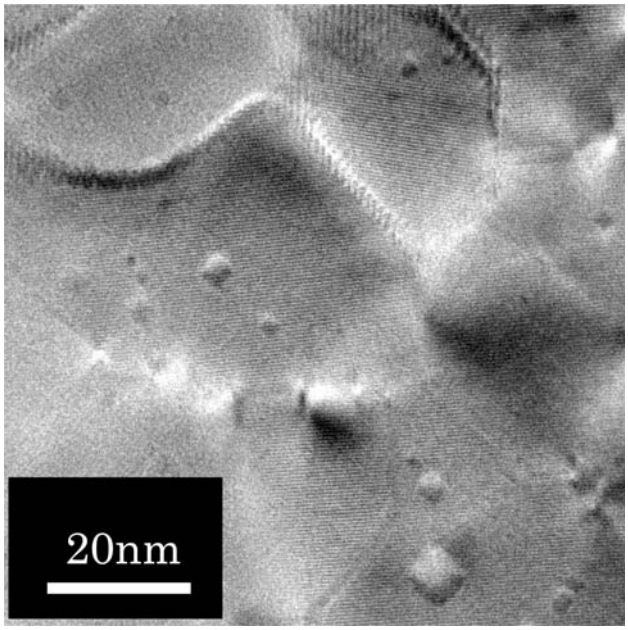


**Fig. 9** TEM micrograph of the $Y_2O_3$ nanosheets obtained by heat treatment at 900 °C for 1 h in air

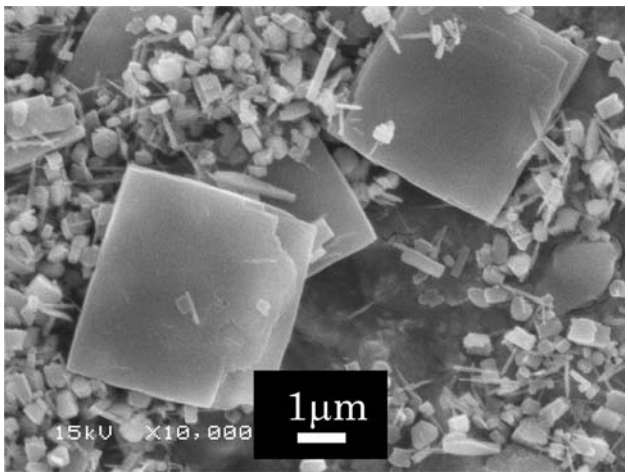


**Fig. 10** SEM micrograph of the sample synthesized under a YIP concentration of 3.75 mol/L

nuclei increased with increasing source concentration. It is thought that this may be an instance of heterogeneous concentration distribution, where small particles disappeared and large particles grew as a result of Oswald ripening.

Figure 11 shows the room temperature emission spectra of $Y(OH)_3$:Eu samples with and without EGME under 397-nm excitation. The peak at 592 nm is due to the allowed magnetic dipole transition ($^5D_0$–$^7F_1$), while the peak at 615 nm is due to the forced electric dipole transition ($^5D_0$–$^7F_2$). The peaks at 651 and 697 nm are attributable to $^5D_0$–$^7F_3$ and $^5D_0$–$^7F_4$ transitions. It can be observed that the

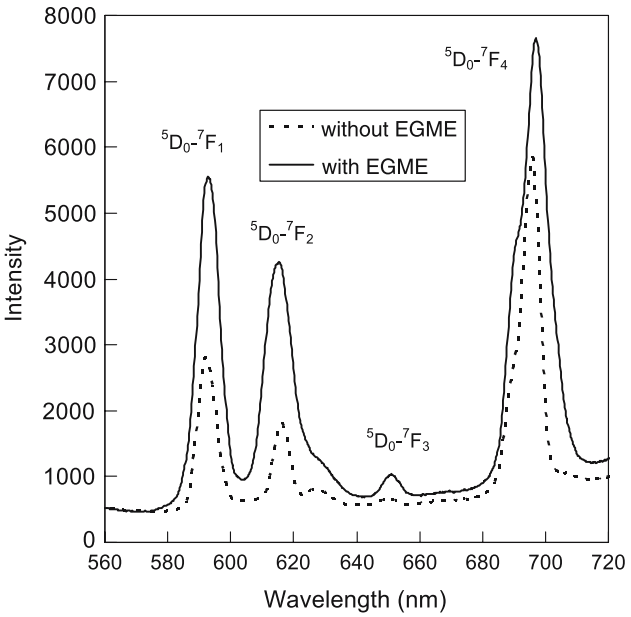


**Fig. 11** The emission spectrum of as-prepared $Y(OH)_3$:Eu excited by 397 nm. Dotted line: synthesized without EGME; solid line: synthesized with EGME

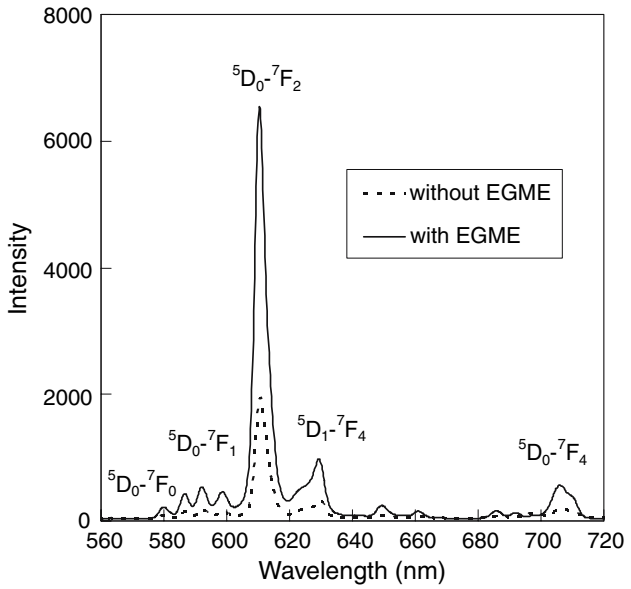


**Fig. 12** The emission spectrum of pre-heated $Y_2O_3$:Eu excited by 467 nm. Dotted line: synthesized without EGME; solid line: synthesized with EGME

main emission intensity was greater than that of the sample without EGME. Figure 12 shows the room temperature emission spectra of $Y_2O_3$:Eu samples with and without EGME under 467-nm excitation. The strongest peak appearing at 611 nm was attributed to the forced electric dipole transition ($^5D_0$–$^7F_2$). Highly forbidden transition peaks can be seen at 580 nm, and the peaks at 587, 592 and 599 nm are due to the magnetic dipole transition ($^5D_0$–$^7F_1$). The main emission intensity is greater than that of the sample without EGME. This is presumably because the yttrium compounds were doped with a higher concentration of Eu ions during the reaction in the solution than the sample without EGME. Another reason was that the surface area of the nanosheets was lower than that of the nanoparticles. The nanosheets become depleted in hydroxyl groups in the immediate vicinity of the $Eu^{3+}$ ions. This reveals the sensitivity of $Eu^{3+}$ fluorescence to the environment, which is attributed to the higher non-radiative path [25]. Thus, the luminescence intensity of the sample with EGME was increased.

## Conclusions

We have successfully developed a route based on EGME acting as template for the hydrothermal synthesis of $Y(OH)_3$ nanosheets. By heat treatment of the $Y(OH)_3$ at 900 °C for 1 h, cubic $Y_2O_3$ nanosheet particles with a thickness of several tens of nanometers and a size of 1 μm could be obtained. More importantly, luminescence intensity from these nanosheets was greater than the rod-like particles synthesized without EGME.

## References

1. Ronda CR (1995) J Alloy Compd 225:534
2. Jing X, Ireland T, Gibbons C (1999) J Electrochem Soc 146:4654
3. Kim CH, Kwon II E, Park CH, Hwang YJ, Bae HS, Yu BY, Pyun CH, Hong GY (2000) J Alloy Compd 311:33
4. Sordelet D, Akinc M (1988) J Colloid Interf Sci 122:47
5. Ikegami T, Li J, Mori T (2002) J Am Ceram Soc 85:1725
6. Huang H, Xu GQ, Chin WS, Gan LM, Chew CH (2002) Nanotechnology 123:318
7. Dhanaraj J, Janannathan R, Kutty TRN, Lu CH (2001) J Phys Chem B 105:11098
8. Tomaszewski H, Weglarz H, Gryse RD (1997) J Euro Ceram Soc 17:403
9. Davolos MR, Feliciano S, Pires AM, Marques RFC, Jafelicci M Jr (2003) J Solid State Chem 171:268
10. Konrad A, Fries T, Gahn A, Kummer F, Herr U, Tidecks R, Samwer K (1999) J Appl Phys 86:3129
11. Kang YC, Roh HS, Park SB (2001) J Am Ceram Soc 84:447
12. Camenzind A, Strobel R, Pratsinis SE (2005) Chem Phys Lett 415:193
13. Tao Y, Zhao G, Zhang W, Xia S (1997) Mater Res Bull 32:501
14. Mckittrick J, Shea LE, Bacalski CF, Bosze EJ (1999) Displays 19:169
15. Kimura T, Kanazawa T, Yamaguchi T (1983) J Am Ceram Soc 66:597
16. Feng Q, Hirasawa M, Yanagisawa K (2001) Chem Mater 13:290
17. El-Toni AM, Yin S, Sato T (2006) Mater Lett 60:185
18. Fang YP, Xu AW, You LP, Song RQ, Yu JC, Zhang HX, Li Q, Liu HQ (2003) Adv Funct Mater 13:955
19. Nishide T, Shibata M (2001) J Sol-Gel Sci Tech 21:189

20. Inoue M, Kondo Y, Inui T (1988) Inorg Chem 27:215
21. Sato T, Imaeda S, Sato K (1988) Thermochimica Acta 133:79
22. Sharma PK, Jilavi MH, Varadan VK, Schmidt H (2002) J Phys Chem Solids 63:171
23. Tang Q, Liu Z, Li S, Zhang S, Liu X, Qian Y (2003) J Cryst Growth 259:208
24. Xu AW, Rang YP, You LP, Liu HQ (2003) J Am Chem Soc 125:1494
25. Devlin K, O'kelly B, Tang ZR, Mcdonagh C, Mcglip (1991) J Non-Cryst Solids 135:8